Applied Catalysis B: Environmental 245 (2019) 114–121

Contents lists available at ScienceDirect

Applied Catalysis B: Environmental

journal homepage: www.elsevier.com/locate/apcatb

Stable, carrier separation tailorable conjugated microporous polymers as a platform for highly efficient photocatalytic H_2 evolution

ARTICLE INFO

Keywords:
Conjugated microporous polymers
Donor-acceptor units
Charge separation
Light absorption
Photocatalytic H_2 production

ABSTRACT

The molecular design of highly photo-functional polymers with high charge separation efficiency and wide spectral absorption are long term quest for photocatalysis. Herein, we design and develop a series of nitrogen-containing conjugated microporous polymers (*N*-CMPs) with tailored donor-acceptor units for enhancing charge separation and light harvesting for visible light photocatalytic H_2 production. By alternating the substitution position (o-, m-, or p-) and the number of electron donor (carbazole, diphenylamine) and acceptor (cyano) units on the 3D-core structure, a series of *N*-CMPs with adjustable donor-acceptor (D-A) charge separation efficiencies and tuneable band gaps in the range of 1.64–2.29 eV were obtained, enabling the precise control of the photocatalytic activity at the molecular level. The optimized *N*-CMP (4-CzPN) exhibits a higher visible light H_2 production rate at 2103.2 μmol/h·g and the apparent quantum yield (AQY) at 420 nm reaches 6.4%. Furthermore, the 4-CzPN photocatalyst maintains excellent durability and recycling performance under 25 h continued light irradiation. The outstanding photocatalytic performance of the optimized *N*-CMPs with D-A structure is attributed to the enhanced polarity and conjugated degree of their core structure, which promotes charge separation and light absorption.

1. Introduction

Inefficient charge separation and limited light absorption range are two critical issues in photocatalysis, which heavily restricts the performance of solar-light photocatalytic hydrogen evolution. Recently, organic semiconductors, possessing many merits compared to inorganic materials (i.e., wide light absorption, low-toxicity, metal-free, structural diversity, etc.), have emerged as promising visible-light photocatalysts and gained much attentions [1–4]. However, due to the inherent characteristics of high exciton binding energy and low crystallinity of organic materials, the mobility and charge separation efficiency of photogenerated carriers are very low, resulting in far below photocatalytic quantum efficiency than inorganic materials. Among many reported organic materials, polymeric carbon nitrides (PCN) have been widely explored as one of the most powerful organic photocatalysts for visible-light photocatalytic H_2 evolution. However, the limited light absorption range until ~460 nm of PCN severely restricts the use of solar energy, whereas 45% and 50% of the solar light are comprised by visible light and near infrared light, respectively [5–7]. Further, the synthesis and modification of PCN often requires a complicated and high-temperature processes, which offers a relatively limited scope for the precise-controlling of structures and properties; the highly effective PCN-based photocatalysts with broad light absorption are often difficult to obtain [8]. To this end, the design and development of novel organic-photocatalysts with high charge separation efficiency and wide light harvesting are still highly needed.

Conjugated microporous polymers (CMPs), a class of π-conjugated porous polymers with a high surface area and structural flexibility, provide a new type of valuable platform for designing photocatalysts with highly efficient charge separation and light absorption [9–11]. In 2015, Cooper A. group developed pyrene-based CMPs photocatalysts with tunable optical gap but the best H_2 evolution rate is only 17.4 μmol/h under visible light [12]. They also synthesized fluorene-based CMPs which showed an AQY of 2.3% at 420 nm but with limited light absorption (~460 nm) [13,14]. Recently, bipyridyl-containing porous conjugated polymer and perylene-containing CMPs photocatalysts have been explored for visible light hydrogen production [15–17]. However, these new-fangled CMPs photocatalysts are still suffering from low charge separation and limited light absorption, thus resulting in low AQY. Bioinspired D-A systems can significantly increase the efficiency for the exciton dissociation and allow charge transfer to overcome the limit of the charge diffusion length of conjugated polymers [18–20]. Due to the conjugated structures and polarity units in CMPs, the photogenerated electrons can rapidly transfer to the acceptor (electron withdrawing groups), while the photogenerated holes simultaneously progress in donor (electron donating units), leading to efficient charge separation [21,22]. On the other hand, the strong orbital interactions between donor and acceptor moieties enhances the double bond character among the repeating units, which enhances the conjugation of the polymer at the molecular scale, thus narrow the band gap and extend the visible light absorption [23]. These two shining features of CMPs provide an alternative approach to construct highly efficient photocatalysts. Current, CMPs with tunable D-A structure are often constructed by co-polymerization of different monomers [19,20,24–26]. For example, Zhang reported a facile approach to fine-tune the redox potentials of CMPs by copolymerizing carbazolic electron donor and electron acceptor based comonomers at different ratios for photocatalytic degradation of lignin [24]. Herein, we report the rational design and synthesis of a series of nitrogen containing-CMPs (*N*-CMPs) constructed by $FeCl_3$-promoted oxidative coupling polymerization using a single monomer with well-tailored D-A units for efficient visible-light-promoted H_2 evolution. Since the *N*-CMPs are

https://doi.org/10.1016/j.apcatb.2018.12.007
Received 22 September 2018
Available online 19 December 2018

composed of repeat units of monomer, the inherent physicochemical and optoelectronic properties of the monomer could be incorporated into the polymers to a great extent. The largely extension of conjugated system and 3D-rigid structure further endows these *N*-CMPs larger surface area, higher porosity, broader light absorption and higher stability compared to their monomer. Thus, the inherent characters and photocatalytic performance of *N*-CMPs herein are designed and fine-tuned by alternating the substitution position and the number of electron donor (carbazole, Cz; diphenylamine, Ph_2N) and acceptor (cyano, CN) units, furnishing the optimized *N*-CMP with high visible light H_2 production rate (2103.2 μmol/h·g) and high apparent quantum yield (420 nm reaches 6.4% AQY at 420 nm). This work unveiled that enhancing the polarity of the *N*-CMPs by optimizing the monomers' D-A property could remarkably promote charge separation and light absorption, and thus increase the photocatalytic H_2 production activity.

2. Results and discussions

We describe the CN-modified *N*-CMP as a versatile design platform to construct efficient polymer photocatalysts. The structural and semiconducting properties of *N*-CMPs can be fine-tuned at the molecular level by alternating the position and numbers of donor and acceptor units in the core structure, as shown in Fig. 1. Carbozole-cyanobenzene monomers (CzCNBs) prepared by a reported one-step nucleophilic substitution reaction of carbazole (diphenylamine) and fluorinated aryl nitrile were chosen as monomers [27,28]. The oxidative coupling polymerization of CzCNBs was readily performed by using anhydrous $FeCl_3$ in trichloroethane ($CHCl_3$) under nitrogen protection. The synthetic details and characterization data are described in the Experimental Section and Supporting Information. The obtained *N*-CMPs with different numbers and positions of Cz and CN groups are referred to as the 4-CzPN, 4-CzIPN, 4-CzTPN, 5-CzBN and 2-CzPN CMPs (Fig. 1). To precisely investigate the influence of the electron donors, a stronger electron donor (diphenylamine, Ph_2N) group [29] is also introduced, which is referred to as 4-DPAPN CMP.

The morphologies of monomers and *N*-CMPs were analysed by scanning electron microscopy (SEM). The representative SEM images of the 4-CzPN monomer and 4-CzPN CMP are shown in Fig. 2a-b, which illustrated the different morphologies before and after polymerization, respectively. The monomer presented a solid block structure, while the *N*-CMP appeared as a flake-like feature with a thickness of less than 100 nm. The morphologies of other *N*-CMPs were also examined (SEM, Figure S2). 4-CzIPN and 4-CzTPN exhibited a porous fibre-like and fused irregular honeycomb shape, and 5-CzBN showed a flake-like

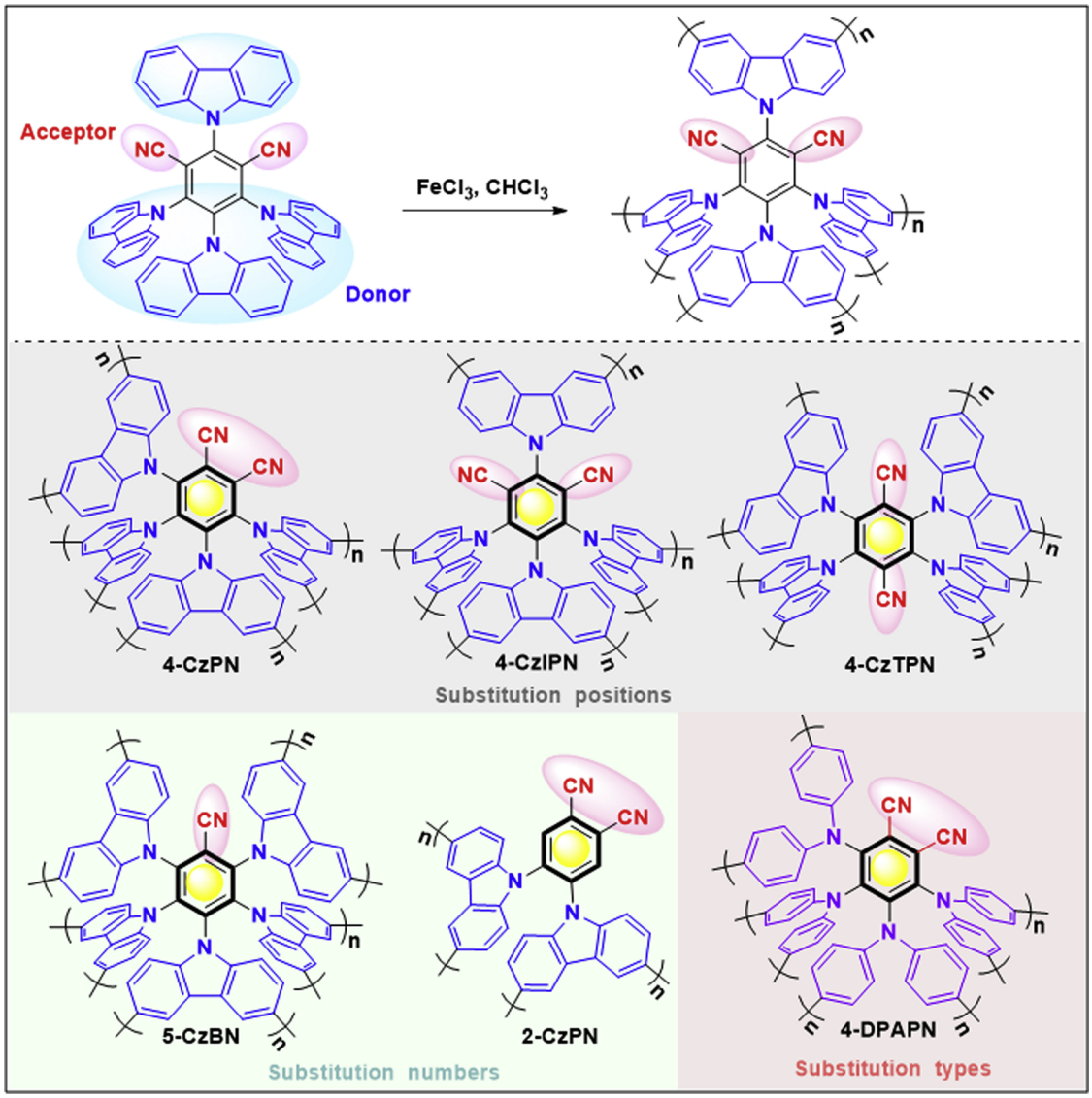

Fig. 1. Molecular structural design of the CN-modified *N*-CMPs by altering the substitution positions, numbers and types on the phenyl group.

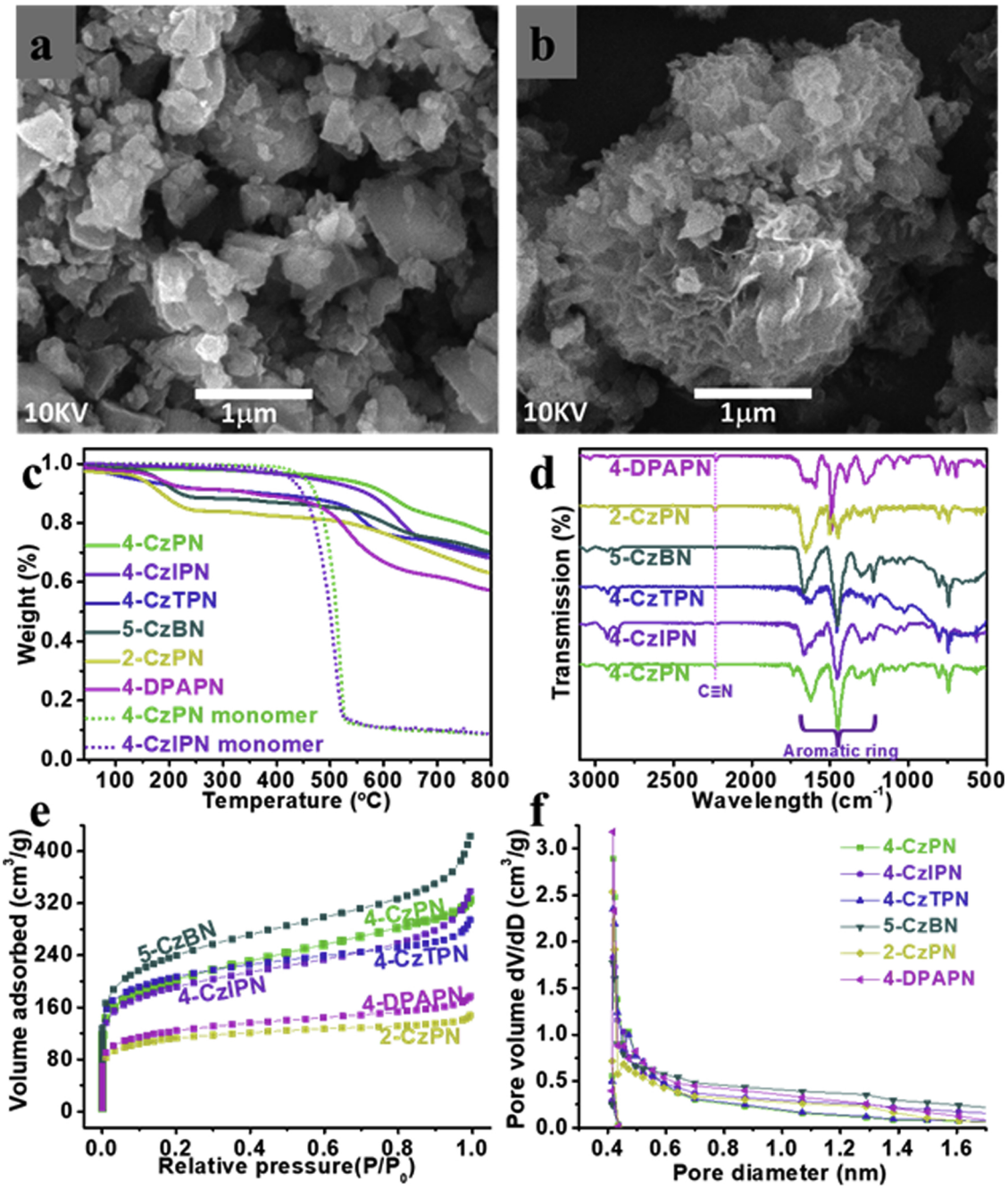

Fig. 2. SEM images of the 4-CzPN monomer (a) and *N*-CMP (b). The thermogravimetric analysis of *N*-CMPs and monomers (c). The FTIR spectra (d), N_2 adsorption isotherms (e) and pore size distributions (f) of six *N*-CMPs with D-A structure.

structure, while 2-CzPN and 4-DPAPN showed a similar rod-shaped structure of particles. The X-ray diffraction (XRD) patterns of the monomers showed good crystallinity, but no sign of crystallinity was exhibited from the corresponding *N*-CMPs (Figure S3). Thermal gravimetric analysis suggests that the thermal stability was remarkably improved after polymerization (TGA, Fig. 2c). The Fourier transform infrared (FTIR, Fig. 2c) spectra showed typical signals at 1393, 1437 and 1655 cm^{-1}, which can be assigned to the skeleton vibration of the aromatic rings in the *N*-CMPs [30]. The signals at 2227 cm^{-1} can be assigned to the C≡N stretching modes. The Brunauer–Emmett–Teller (BET) surface area and pore size distribution of the CN-modified *N*-CMPs were characterized using N_2 adsorption isotherms. As shown in Fig. 2e–f, a type-I isotherm was presented in all synthesized CMPs, and the pore diameters were approximately 0.45 nm in the pore size distribution curve, indicating a typical micropore structure in *N*-CMPs [31]. The BET surface areas of the 4-CzPN, 4-CzIPN, 4-CzTPN, 5-CzBN, 2-CzPN and 4-DPAPN CMPs were measured to be 692.5, 648.6, 691.9, 818.8, 374.8 and 416.2 m^2/g, with total pore volumes of 0.3178, 0.3341, 0.2255, 0.4315, 0.0994 and 0.1396 cm^3/g, respectively (Fig. 2e and f), and a similar pore diameters distribution was observed for all these *N*-CMPs. These results indicate that the 3D-structure and porosity can be regulated by the number of Cz groups on the core-benzene-ring, the more Cz groups, the larger the BET surface areas and pore volumes.

The *N*-CMPs were synthesized by $FeCl_3$-promoted oxidative polymerization using a single monomer. Thus, the inherent property of monomers can be maintained to great extent. In principle, the greatly extended conjugated system could endow these materials with significantly improved surface area, porosity, stability and light absorption

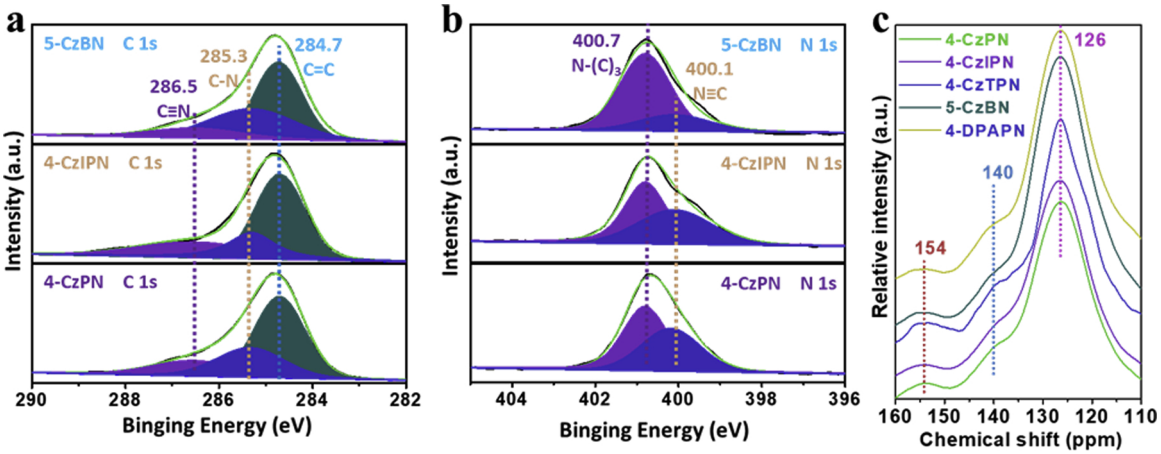

Fig. 3. The C 1s XPS spectra (a) and N 1s (b) of 4-CzPN, 4-CzIPN and 5-CzBN CMPs. Solid state CP/MAS ^{13}C NMR spectra (c) of 4-CzPN, 4-CzIPN, 4-CzTPN, 5-CzBN and 4-DPAPN CMPs.

[9,24]. The elemental analysis, XPS and solid-state CP/MAS, ^{13}C NMR characterizations was adopted to determine the synthesized structures of six *N*-CMPs with D-A structure. Elemental analysis (Table S1) showed that the weight ratio of the C, N and H elements were 85% ~ 88%, 9% ~ 11% and 3% ~ 5%, well- matching with the chemical formulas (4-CzPN, $(C_{56}N_6H_{24})_n$; 4-CzIPN, $(C_{56}N_6H_{24})_n$; 4-CzTPN, $(C_{56}N_6H_{24})_n$; 5-CzBN, $(C_{67}N_6H_{30})_n$; 2-CzPN, $(C_{32}N_4H_{14})_n$; 4-DPAPN, $(C_{56}N_6H_{32})_n$). The X-ray photoelectron spectra (XPS) of D-A-modified *N*-CMPs are shown in Fig. 3a and b. The C 1 s spectra can be de-convoluted into three peaks, which are attributed to the C≡N bonds (286.5 eV), C–N bonds (285.3 eV) [32] and C═C bonds in aromatic rings (284.7 eV) [33]. The N 1 s spectra are assigned to N-$(C)_3$ (400.7 eV) and N≡C (400.1 eV) [7]. With the increase in the number of Cz and the decrease in the number of CN groups, the significant changes in peak intensity at 400.7 eV and 400.1 eV were observed in 5-CzBN CMP. Solid state CP/MAS ^{13}C NMR spectra (Fig. 3c) reveal three broad resonance peaks at 154, 140 and 126 ppm for these *N*- CMPs [34]. Specifically, the peak at 154 ppm can be attributed to C atoms in CN groups and the peak at 140 ppm are aryl C atoms next to the carbazolic N atoms [24]. The peak at 126 ppm corresponds to the unsubstituted aryl C atoms and its intensity increases significantly in 5-CzBN CMP. These characterizations may indirectly explain the structure of the polymer.

The band gaps of the CN-modified *N*-CMPs can be narrowed by the strong orbital interactions between donor and acceptor moieties. The adjustable colours of these *N*-CMPs, as shown in Fig. 4a, changed from yellow to black vividly demonstrated that the band gaps of these *N*-CMPs can be adjusted in a broad range. The ultraviolet-visible diffuse reflectance spectra (UV–vis DRS, Fig. 4b) revealed that the *N*-CMPs showed a broad absorption from 600 to 900 nm. The 4-DPAPN CMP exhibited the largest adsorption area among all the *N*-CMPs, which even capture the light up to the near-infrared region (900 nm), while 5-CzBN showed the narrowest absorption range. The bandgaps (E_g) of these *N*-CMPs are in the range of 1.64–2.27 eV (Fig. 4c). Apparently, the relatively wide distribution of E_g could be simply achieved by changing the number of electron donors and acceptors, the positions of the acceptors (o-, m-, or p-), and the nature of the electron donors (Cz or Ph_2N). 4-DPAPN CMP has a narrowest band gap (1.64 eV) among six *N*-CMPs due to stronger electron donating characteristics of Ph_2N than that of Cz. Cyclic voltammetry (CV) measurements (Figure S4) were conducted to further measure the lowest unoccupied molecular orbital (LUMO) positions of the *N*-CMPs. The highest occupied molecular orbital (HOMO) positions could be derived by adding the E_g to the LUMO value. In Fig. 4d, the different HOMO and LUMO energy levels of these *N*-CMPs were presented, and the LUMO positions were much higher than the potentials of H^+/H_2 (0 V, pH = 0). These energy levels reached the thermodynamic conditions for photocatalytic H_2 production.

The photocatalytic activity of these obtained *N*-CMPs for H_2 evolution was tested under visible light irradiation ($\lambda > 420$ nm, UVCUT-420 nm filter, Figure S5). All the *N*-CMPs showed a steady and molecular structure dependent H_2 production rate (Fig. 5a). Specifically, 4-CzPN and 2-CzPN exhibited the highest H_2 production rate of 2103.2 and 1558.4 μmol/h·g; 4-CzIPN and 5-CzBN demonstrated moderate rates of 1273.4 and 606.1 μmol/h·g; and 4-CzTPN and 4-DPAPN showed the lowest rates of 188.2 and 129.8 μmol/h·g, respectively. For comparison, the most well-known PCN prepared from urea was tested under the same conditions. The absorption of PCN (Figure S6b) reached up to 462 nm, which is far less than that exhibited by the *N*-CMPs with D-A structure. Particularly, 4-CzPN exhibited two times higher visible light H_2 production rate than PCN. More than 25 h continuous hydrogen evolution test demonstrates almost no decline in activity (Fig. 5c). The overall photocatalytic performance and stability characteristics of 4-CzPN were much better than most of the reported polymer photocatalysts such as soluble polycarbazole [35], pyrene-based CMPs [12], phenyl-triazine oligomers [37], crystalline polyimide [40], poly(azomethine) [41] and triazine-based frameworks (Fig. 5e) [42]. Its apparent quantum yield (AQY) is about 6.4% at 420 nm, which is the relatively high values among the reported CMPs as well as other newfangled polymer photocatalysts; even at 700 ± 10 nm, the AQY is still as high as 0.05%. Furthermore, the XRD, UV − Vis DRS and FTIR spectra of 4-CzPN before and after a photocatalytic reaction showed no obvious signs of photodegradation (Figure S7), indicating their excellent structure stability. Fig. 5d proposed the mechanism of the photocatalytic H_2 production by the *N*-CMPs, whereas the cocatalysts Pt nanoparticles were reduced by the photogenerated electrons from 4-CzPN and *in-situ* anchored onto the surface (Figure S8). As a sacrificial reagent, triethanolamine (TEOA) can rapidly capture photogenerated holes and be oxidized into $TEOA^+$ [45,46]. Since the LOMO position is 0.82 V higher than that of H^+/H_2 (0 V), the photogenerated electrons in 4-CzPN CMPs can easily transfer to Pt nanoparticles and have enough reducing capacity to react with H_2O, to produce H_2 on the surface of Pt nanoparticles.

To gain more insight into the linkage between the molecular structural differences and photocatalytic activity, the steady-state photoluminescence (PL), time-resolved photoluminescence (TRPL) spectra and visible-light photocurrent were examined. In Fig. 6a, a strong PL emission peak located at approximately 540 nm is observed for 4-CzTPN, which may be attributed to the recombination radiation of photoinduced charge carriers and excitons. Although the position of the emission peaks of 4-CzPN, 4-CzIPN and 2-CzPN sample is same as that

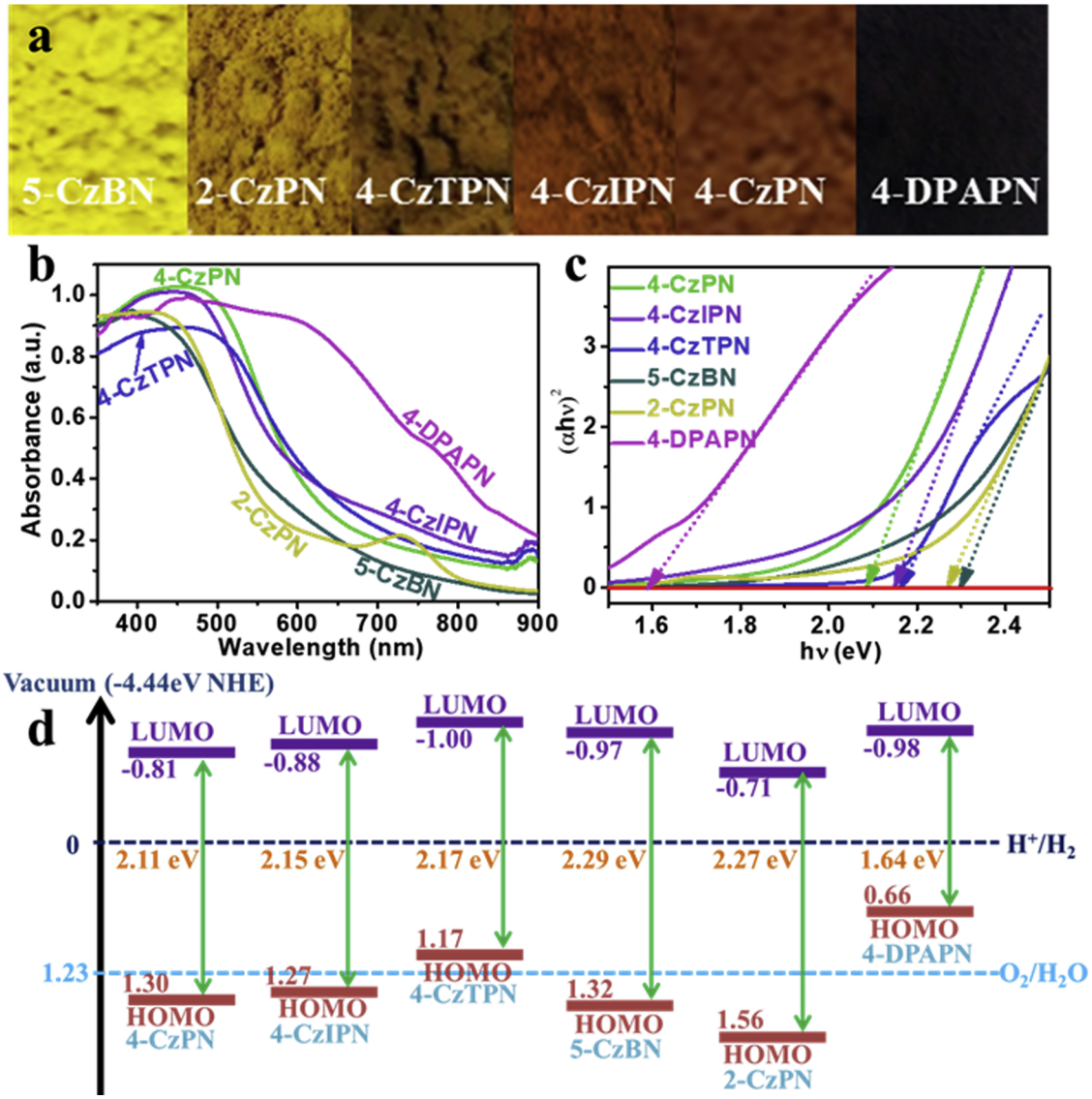

Fig. 4. The optical images (a), UV–vis DRS spectra (b), Tauc plots of the transformed Kubelka-Munk function *vs*. the energy (c) and the energy level positions (d) of six CN-modified *N*-CMPs.

of 4-CzTPN, the PL emission intensity is drastically reduced. The fluorescence is even quenched in the case of 4-CzPN. This phenomenon indicates the much higher charge separation efficiency of 4-CzPN than that of 4-CzTPN and 4-CzIPN, which is well consistent with the observation that 4-CzPN has a higher H_2 evolution rate than that of 4-CzIPN and 4-CzTPN. 4-DPAPN with stronger electron-donating (Ph_2N) characteristics exhibits a very narrow bandgap (1.64 eV) and a high fluorescence emission peak located at approximately 610 nm (Fig. 6a). This result suggests that the poor photocatalytic performance of 4-DPAPN is probably caused by the fast recombination of photogenerated charge carriers and inefficient charges separation. Further, the charge transfer dynamics was investigated by TRPL decay spectra. In Fig. 6b, the average lifetime of photogenerated electrons in 4-CzPN (2.65 ns) is strikingly longer than that of other *N*-CMPs, indicating a longer lifetime of photoexcited excitons or slower recombination of electron-hole pairs, which demonstrated that more separated photoexcited electrons can be more efficiently separated and therefore shown higher photoreactivity in H_2 evolution. The visible-light photocurrent characterization (Fig. 6c) was added to further investigate the charge separation of six CN-modified *N*-CMPs. When the visible light is successively shuttled on and off, a series of photocurrent signals can be detected. The strength of the photocurrent was matched well with the PL, TRPL and photocatalytic activity. Since the inherent optoelectronic properties could be maintained in *N*-CMPs, we next calculated the distributions of the frontier orbitals in monomers as models using DMol3 to reveal the D-A properties in *N*-CMPs. Fig. 6c-d and S9-S13 show the calculated HOMO and LUMO of the monomers. All the monomers present a strong D-A property and separated HOMO and LUMO orbits. The HOMO orbits are mainly populated along the Cz groups, while the LUMO orbits are largely localized among the CN units. The superposition and counteraction effect originated from the position of CN groups has an important influence on monomers' D-A characteristics. For example, 4-CzPN and 2-CzPN present the strongest D-A property, 4-CzTPN and 5-CzBN express the moderate D-A property. What's more, for 4-CzPN with the ortho substitution of two CN groups, the superposition of electron-withdrawing property results in the inhomogeneous distribution of HOMO orbits on two of the four Cz groups. The HOMO orbits in 5-CzBN are in homogeneously populated along four of the five Cz groups because of the electron-withdrawing property of one CN group. On the contrary, for 4-CzTPN with the para substitution of two CN groups, the HOMO orbits are averagely localized among the four CZ groups due to the counteraction of electron-withdrawing property. In addition, due to the

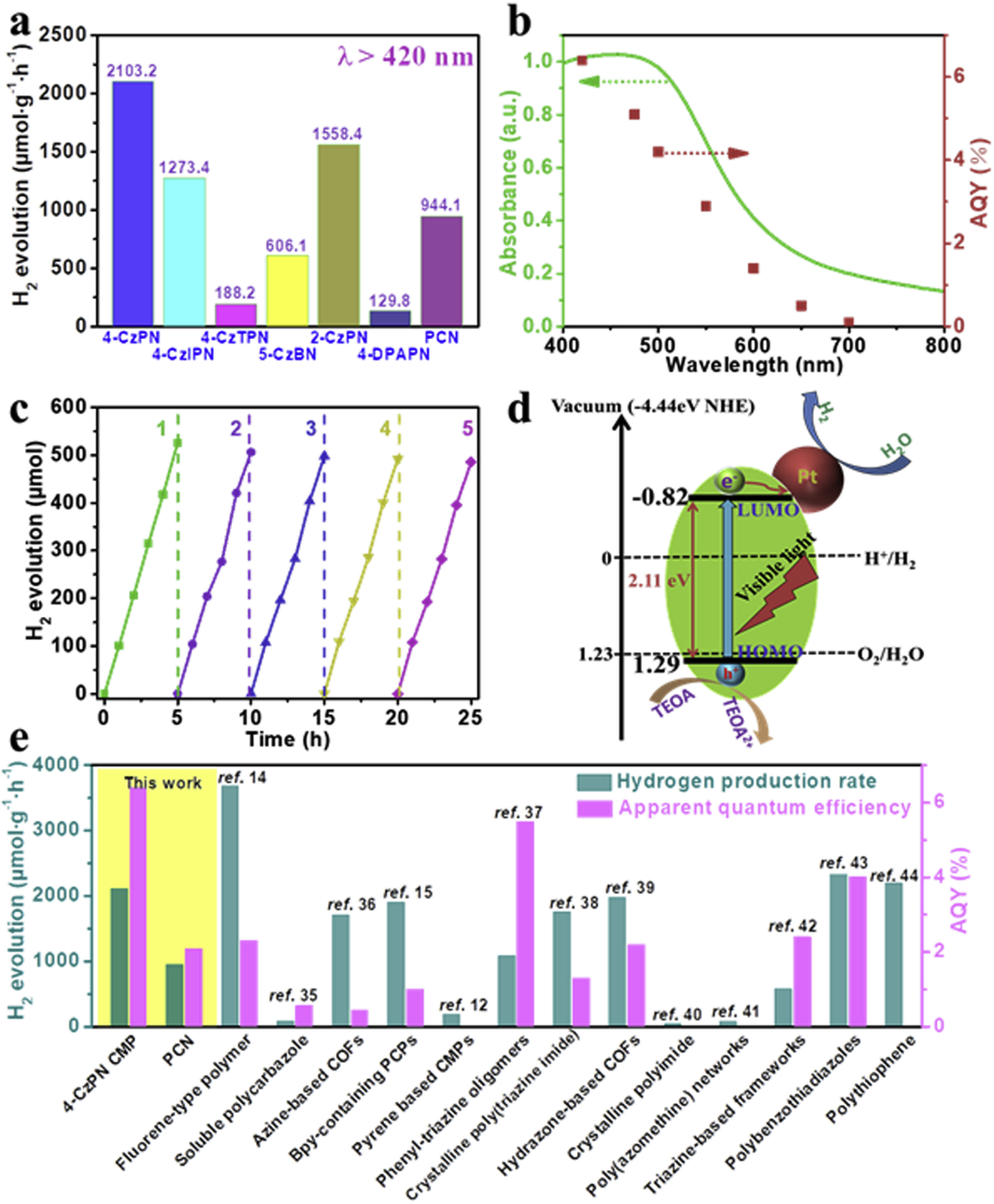

Fig. 5. Normalized H_2 production rate (a) of six CN-modified *N*-CMPs and PCN under visible light (λ > 420 nm) irradiation. The AQY with wavelength change (b), recycling measurements of the H_2 production (c) and photocatalytic schematic diagram (d) of 4-CzPN CMP. Comparison of 4-CzPN CMP with other reported polymers towards photocatalytic H_2 production (e). The 50 mg of obtained CN-modified *N*-CMPs loaded with 3.0 wt% Pt was placed into a TEOA solution (150 mL of deionized distilled water, 30 mL of TEOA) in a closed gas circulation system [36,38,39,43,44].

conjugated structures and polarity units in the *N*-CMPs, the photogenerated electrons can rapidly transfer to the LUMO orbits localized among the CN groups, while the photogenerated holes simultaneously progress in the opposite direction populated among the Cz groups, leading to efficient charge separation (Fig. 6e). Engineering the donor and acceptor units and extending polarity in the core structure of the *N*-CMPs can decrease the coulombic binding energy for dissociating electron-hole pairs and hence increase the charge separation [21,22].

3. Conclusions

In conclusion, highly efficient visible-light-active *N*-CMPs were successfully prepared by rationally designing and modulating the donor-acceptor functional groups for enhancing charge separation and light absorption. The advantages of self-polymerization strategy in construction of the carrier-separation tailorable and photoactive *N*-CMPs are now much clearer: 1) the distribution of D-A is homogenous

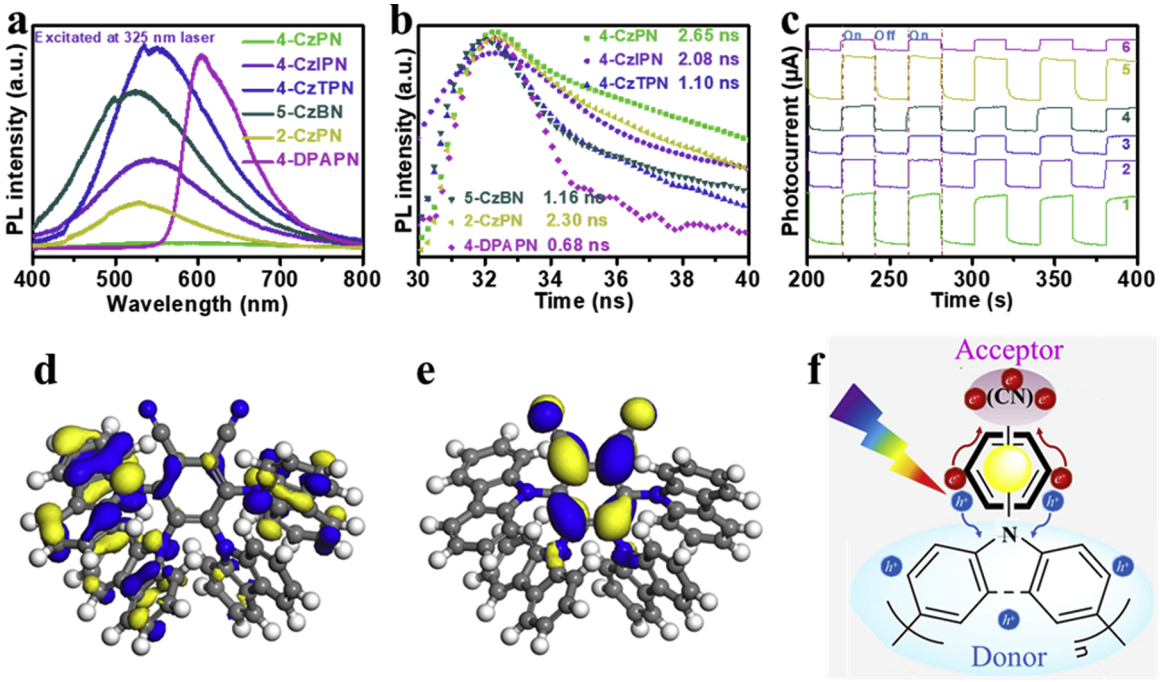

Fig. 6. The fluorescence (a) and time-resolved fluorescence spectra (b) of the six CN-modified *N*-CMPs. The visible-light photocurrent (c) of *N*-CMPs (1, 4-CzPN; 2, 4-CzIPN; 3, 4-CzTPN; 4, 5-CzBN; 5, 2-CzPN; 6, 4-DPAPN). The electronic density distribution of HOMO (d) and LUMO (e) of 4-CzPN. Schematic diagram of CN-modified *N*-CMPs under light excitation (f).

and the ratio of D-A is unequivocal in the *N*-CMPs composed of repeat units of monomer; 2) the E_g values, 3D-rigid skeleton, porosity, light absorption ranges and charge separation efficiencies of *N*-CMPs could be well-designed at molecular-level by simply alternating the monomers; 3) the superposition and substitution effect originated from the position of CN groups in monomers could be maintained in *N*-CMPs, which determinates their charge-separation efficiency and photocatalytic reactivity. As a result, the screened *N*-CMP with optimized structure and properties show excellent visible light H_2 production rate at 2103.2 μmol/h·g and high apparent quantum yield (AQY) (6.4% at 420 nm). This study has tremendous implication for the development highly efficient photocatalysis for water splitting and artificial photosynthesis. The full potential of these *N*-CMP materials and their derivatives for overall water splitting and artificial photosynthesis of fine chemicals and pharmaceutical-related compounds are currently undergo in our lab.

Acknowledgements

This work was jointly supported by the Natural Science Foundation of China (21761142011, 51502174, 21401190), Science and Technology Project of the Research Foundation of China Postdoctoral Science (2018M630982, 2017M612710, 2016M592519), the Shenzhen Peacock Plan (Grant No. 827-000113, KQJSCX20170727100802505, KQTD20160531120429 71), the Educational Commission of Guangdong Province (2016KCXTD006 and 2016KSTCX126), Science and Technology Project of Shenzhen (ZDSYS201707271014468), Shenzhen Innovation Program (JCYJ 20170818142642395), Guangdong Special Support Program and the Singapore National Research Foundation via the grant of NRF2017NRF-NSFC001-007.

Appendix A. Supplementary data

Supplementary material related to this article can be found, in the online version, at doi:https://doi.org/10.1016/j.apcatb.2018.12.007.

References

[1] Y.-Z. Long, M.-M. Li, C. Gu, M. Wan, J.-L. Duvail, Z. Liu, Z. Fan, Recent advances in synthesis, physical properties and applications of conducting polymer nanotubes and nanofibers, Prog. Polym. Sci. 36 (2011) 1415–1442.
[2] S. Allard, M. Forster, B. Souharce, H. Thiem, U. Scherf, Organic semiconductors for solution-processable field-effect transistors (OFETs), Angew. Chem. Int. Ed. 47 (2008) 4070–4098.
[3] V.A. Dediu, L.E. Hueso, I. Bergenti, C. Taliani, Spin routes in organic semiconductors, Nat. Mater. 8 (2009) 707–716.
[4] S. Sergeyev, W. Pisula, Y.H. Geerts, Discotic liquid crystals: a new generation of organic semiconductors, Chem. Soc. Rev. 36 (2007) 1902–1929.
[5] X. Wang, K. Maeda, A. Thomas, K. Takanabe, G. Xin, J.M. Carlsson, K. Domen, M. Antonietti, A metal-free polymeric photocatalyst for hydrogen production from water under visible light, Nat. Mater. 8 (2009) 76–80.
[6] J. Zhang, X. Chen, K. Takanabe, K. Maeda, K. Domen, J.D. Epping, X. Fu, M. Antonietti, X. Wang, Synthesis of a carbon nitride structure for visible-light catalysis by copolymerization, Angew. Chem. Int. Ed. 49 (2010) 441–444.
[7] S. Cao, J. Low, J. Yu, M. Jaroniec, Polymeric photocatalysts based on graphitic carbon nitride, Adv. Mater. 27 (2015) 2150–2176.
[8] J. Wen, J. Xie, X. Chen, X. Li, A review on *g*-C_3N_4-based photocatalysts, Appl. Surf. Sci. 391 (2016) 72–123.
[9] C. Su, R. Tandiana, B. Tian, A. Sengupta, W. Tang, J. Su, K.P. Loh, Visible-light photocatalysis of aerobic oxidation reactions using carbazolic conjugated microporous polymers, ACS Catal. 6 (2016) 3594–3599.
[10] Y. Xu, S. Jin, H. Xu, A. Nagai, D. Jiang, Conjugated microporous polymers: design, synthesis and application, Chem. Soc. Rev. 42 (2013) 8012–8031.
[11] A. Bhunia, D. Esquivel, S. Dey, R.J. Fernandez-Teran, Y. Goto, S. Inagaki, P.V.D. Voort, C. Janiak, A photoluminescent covalent triazine framework: CO_2 adsorption, light-driven hydrogen evolution and sensing of nitroaromatics, J. Mater. Chem. A Mater. Energy Sustain. 4 (2016) 13450–13457.
[12] R.S. Sprick, J. Jiang, B. Bonillo, S. Ren, T. Ratvijitvech, P. Guiglion, M.A. Zwijnenburg, D.J. Adams, A.I. Cooper, Tunable organic photocatalysts for visible-light-driven hydrogen evolution, J. Am. Chem. Soc. 137 (2015) 3265–3270.
[13] R.S. Sprick, B. Bonillo, M. Sachs, R. Clowes, J.R. Durrant, D.J. Adams, A.I. Cooper, Extended conjugated microporous polymers for photocatalytic hydrogen evolution from water, Chem. Commun. (Camb.) 52 (2016) 10008–10011.
[14] R.S. Sprick, B. Bonillo, R. Clowes, P. Guiglion, N.J. Brownbill, B.J. Slater, F. Blanc, M.A. Zwijnenburg, D.J. Adams, A.I. Cooper, Visible-light-driven hydrogen evolution using planarized conjugated polymer photocatalysts, Angew. Chem. Int. Ed. 55 (2016) 1792–1796.
[15] L. Li, Z. Cai, Q. Wu, W.-Y. Lo, N. Zhang, L.X. Chen, L. Yu, Rational design of porous conjugated polymers and roles of residual palladium for photocatalytic hydrogen production, J. Am. Chem. Soc. 138 (2016) 7681–7686.
[16] Y. Xu, N. Mao, S. Feng, C. Zhang, F. Wang, Y. Chen, J. Zeng, J.X. Jiang, Perylene-containing conjugated microporous polymers for photocatalytic hydrogen evolution, Macromol. Rapid Commun. 218 (2017).

[17] Y. Xu, C. Zhang, P. Mu, N. Mao, X. Wang, Q. He, F. Wang, J.-X. Jiang, Tetra-armed conjugated microporous polymers for gas adsorption and photocatalytic hydrogen evolution, Sci. China Chem. 60 (2017) 1075–1083.
[18] H. Ou, X. Chen, L. Lin, Y. Fang, X. Wang, Biomimetic donor-acceptor motifs in conjugated polymers for promoting exciton splitting and charge separation, Angew. Chem. Int. Ed. 57 (2018) 8729–8733.
[19] Y. Xu, N. Mao, C. Zhang, X. Wang, J. Zeng, Y. Chen, F. Wang, J. Jiang, Rational design of donor-π-acceptor conjugated microporous polymers for photocatalytic hydrogen production, Appl. Catal. B: Environ. 228 (2018) 1–9.
[20] Y. Xiang, X. Wang, L. Rao, P. Wang, D. Huang, X. Ding, X. Zhang, S. Wang, H. Chen, Y. Zhu, Conjugated polymers with sequential fluorination for enhanced photocatalytic H_2 evolution via proton-coupled Electron transfer, ACS Energy Lett. 3 (2018) 2544–2549.
[21] A.J. Zucchero, P.L. McGrier, U.H. Bunz, Cross-conjugated cruciform fluorophores, Acc. Chem. Res. 43 (2009) 397–408.
[22] H.C. Zhang, E.Q. Guo, Y.L. Zhang, P.H. Ren, W.J. Yang, Donor-acceptor-substituted anthracene-centered cruciforms: synthesis, enhanced two-photon absorptions, and spatially separated frontier molecular orbitals, Chem. Mater. 21 (2009) 5125–5135.
[23] A. Ajayaghosh, Donor-acceptor type low band gap polymers: polysquaraines and related systems, Chem. Soc. Rev. 32 (2003) 181–191.
[24] J. Luo, X. Zhang, J. Lu, J. Zhang, Fine tuning the redox potentials of carbazolic porous organic frameworks for visible-light photoredox catalytic degradation of lignin β-O-4 models, ACS Catal. 7 (2017) 5062–5070.
[25] L. Li, W. Lo, Z. Cai, N. Zhang, L. Yu, Donor-acceptor porous conjugated polymers for photocatalytic hydrogen production: the importance of acceptor comonomer, Macromolecules 49 (2016) 6903–6909.
[26] K. Kailasam, M. Mesch, L. Möhlmann, M. Baar, S. Blechert, M. Schwarze, M. Schröder, R. Schomäcker, J. Senker, A. Thomas, Donor-acceptor-Type heptazine based polymer networks for photocatalytic hydrogen evolution, Energy Techno. 4 (2016) 744–750.
[27] F. Diness, M. Begtrup, Sequential direct SNAr reactions of Pentafluorobenzenes with azole or indole derivatives, Org. Lett. 16 (2014) 3130–3133.
[28] H. Uoyama, K. Goushi, K. Shizu, H. Nomura, C. Adachi, Highly efficient organic light-emitting diodes from delayed fluorescence, Nature 492 (2012) 234–238.
[29] J. Luo, J. Zhang, Donor-acceptor fluorophores for visible-light-promoted organic synthesis: Photoredox/Ni dual catalytic C (sp^3)-C (sp^2) cross-coupling, ACS Catal. 6 (2016) 873–877.
[30] G. Tian, G. Zhu, X. Yang, Q. Fang, M. Xue, J. Sun, Y. Wei, S. Qiu, A chiral layered Co (II) coordination polymer with helical chains from achiral materials, Chem. Commun. (Camb.) 11 (2005) 1396–1398.
[31] A.I. Cooper, Conjugated microporous polymers, Adv. Mater. 21 (2009) 1291–1295.
[32] J. Jang, C. Lee, Structural study of nitrogen-doping effects in bamboo-shaped multiwalled carbon nanotubes, Appl. Phys. Lett. 84 (2004) 2877–2879.
[33] Y. Mu, N. Wang, Z. Sun, J. Wang, J. Li, J. Yu, Carbogenic nanodots derived from organo-templated zeolites with modulated full-color luminescence, Chem. Sci. 7 (2016) 3564–3568.
[34] Q. Chen, D. Liu, M. Luo, L. Feng, Y. Zhao, B. Han, Nitrogen-containing microporous conjugated polymers via carbazole-based oxidative coupling polymerization: preparation, porosity, and gas uptake, Small 10 (2014) 308–315.
[35] D.J. Woods, R.S. Sprick, C.L. Smith, A.J. Cowan, A.I. Cooper, A solution-processable polymer photocatalyst for hydrogen evolution from water, Adv. Energy Mater. 7 (2017).
[36] V.S. Vyas, F. Haase, L. Stegbauer, G. Savasci, F. Podjaski, C. Ochsenfeld, B.V. Lotsch, A tunable azine covalent organic framework platform for visible light-induced hydrogen generation, Nat. Commun. 6 (2015) 8508.
[37] K. Schwinghammer, S. Hug, M. Mesch, J. Senker, B.V. Lotsch, Phenyl-triazine oligomers for light-driven hydrogen evolution, Energy Environ. Sci. 8 (2015) 3345–3353.
[38] K. Schwinghammer, M.B. Mesch, V. Duppel, C. Ziegler, J. Senker, B.V. Lotsch, Crystalline carbon nitride nanosheets for improved visible-light hydrogen evolution, J. Am. Chem. Soc. 136 (2014) 1730–1733.
[39] L. Stegbauer, K. Schwinghammer, B.V. Lotsch, A hydrazone-based covalent organic framework for photocatalytic hydrogen production, Chem. Sci. 5 (2014) 2789–2793.
[40] S. Chu, Y. Wang, Y. Guo, P. Zhou, H. Yu, L. Luo, F. Kong, Z. Zou, Facile green synthesis of crystalline polyimide photocatalyst for hydrogen generation from water, J. Mater. Chem. 22 (2012) 15519–15521.
[41] M.G. Schwab, M. Hamburger, X. Feng, J. Shu, H.W. Spiess, X. Wang, M. Antonietti, K. Müllen, Photocatalytic hydrogen evolution through fully conjugated poly(azomethine) networks, Chem. Commun. (Camb.) 46 (2010) 8932–8934.
[42] J. Bi, W. Fang, L. Li, J. Wang, S. Liang, Y. He, M. Liu, L. Wu, Covalent triazine-based frameworks as visible light photocatalysts for the splitting of water, Macromol. Rapid Commun. 36 (2015) 1799–1805.
[43] C. Yang, B.C. Ma, L. Zhang, S. Lin, S. Ghasimi, K. Landfester, K.A.I. Zhang, X. Wang, Molecular engineering of conjugated polybenzothiadiazoles for enhanced hydrogen production by photosynthesis, Angew. Chem. Int. Ed. 55 (2016) 9202–9206.
[44] X. Zong, X. Miao, S. Hua, L. An, X. Gao, W. Jiang, D. Qu, Z. Zhou, X. Liu, Z. Sun, Structure defects assisted photocatalytic H_2 production for polythiophene nanofibers, Appl. Catal. B-Environ. 211 (2017) 98–105.
[45] K. Kalyanasundaram, J. Kiwi, M. Grätzel, Hydrogen evolution from water by visible light, a homogeneous three component test system for redox catalysis, Helv. Chim. Acta 61 (1978) 2720–2730.
[46] Z. Chai, Q. Li, D. Xu, Photocatalytic reduction of CO_2 to CO utilizing a stable and efficient hetero-homogeneous hybrid system, RSC Adv. 4 (2014) 44991–44995.

Guoqiang Zhang[a,b,c,1], Wei Ou[a,1], Jun Wang[a], Yangsen Xu[a], Dong Xu[d], Tao Sun[a], Shuning Xiao[a,b], Mengran Wang[a], Hexing Li[e], Wei Chen[b], Chenliang Su[a,c,*]

[a] *SZU-NUS Collaborative Innovation Center for Optoelectronic Science & Technology, International Collaborative Laboratory of 2D Materials for Optoelectronics Science and Technology of Ministry of Education, College of Optoelectronic Engineering, Shenzhen University, Shenzhen 518060, China*

[b] *Department of Chemistry, National University of Singapore, Singapore 117543, Singapore*

[c] *Engineering Technology Research Center for 2D Material Information Function Devices and Systems of Guangdong Province, Shenzhen University, Shenzhen 518060, China*

[d] *Department of Civil and Environmental Engineering, National University of Singapore, Singapore 117576, Singapore*

[e] *The Education Ministry Key Lab of Resource Chemistry, Shanghai Key Laboratory of Rare Earth Functional Materials, Shanghai Normal University, Shanghai 200234, China*

E-mail address: chmsuc@szu.edu.cn (C. Su).

* Corresponding author at: SZU-NUS Collaborative Innovation Center for Optoelectronic Science & Technology, International Collaborative Laboratory of 2D Materials for Optoelectronics Science and Technology of Ministry of Education, College of Optoelectronic Engineering, Shenzhen University, Shenzhen 518060, China.

[1] These authors contributed equally to this work.